QUANTIFICATION OF LONGITUDINAL CHANGES IN RETINAL VASCULATURE FROM WIDE-FIELD FLUORESCEIN ANGIOGRAPHY VIA A NOVEL REGISTRATION AND CHANGE DETECTION APPROACH

Li Ding[1], *Ajay Kuriyan*[2], *Rajeev Ramchandran*[2], *and Gaurav Sharma*[1]

[1]Dept. of Electrical and Computer Engineering, [2]Dept. of Ophthalmology,
University of Rochester, Rochester, NY

ABSTRACT

Wide-field fluorescein angiography (FA) images are commonly used in ophthalmology to assess longitudinal changes in retinal vasculature, specifically, non-perfusion. Current practice relies on manual qualitative comparisons between images taken at successive clinic visits, a few months apart. Objective quantitative assessments, although desirable for evaluating disease progression and treatment, are impractical to perform manually and challenging for image analysis because of the changes in the capture viewpoints and temporal imaging variations seen as the FA dye injection perfuses the retina. We propose a methodology for quantifying retinal non-perfusion by automated analysis of the FA images captured during successive clinical visits. Blood vessels are first detected in the image from each visit. The vascular networks in FA images are then precisely registered to obtain a co-aligned pair via parametric chamfer matching under polynomial transformation, a process that explicitly allows for increase or decrease in perfusion. Changes in perfusion are then quantified by identifying the common and distinct regions in co-aligned image pairs. The proposed framework is tested on FA images that are manually annotated by an ophthalmologist to provide ground truth binary vessel masks and to identify vasculature changes. Results indicate that the proposed method provides assessments of vasculature changes that are in good agreement with the ophthalmologist-provided annotations.

Index Terms— wide-field fluorescein angiography, vessel detection, image registration, expectation maximization (EM)

1. INTRODUCTION

Common systemic diseases, such as diabetes, hypertension, and artherosclerosis affect blood vessels throughout the body [1]. Retinal non-perfusion (RNP), or ischemia, which is a lack of blood flow to the retina, directly results in the most severe blinding complications of systemic diseases in the eye, including proliferative diabetic retinopathy, tractional retinal detachments, vitreous hemorrhage, and neovascular glaucoma. The impact of RNP on the vascular system can be visualized in using wide-field fluorescein angiography (FA), a process that involves injecting fluorescein dye intravenously and taking images that capture the fluorescence of the dye passing through the retinal blood vessels using a fundus camera with suitable optical filters [2]. Figure 1 shows two samples FA images taken for one patient over time[1]. Compared to alternatives such as color fundus images, FA image has the advantage that they provide a wide field of view (FOV). Typically, color fundus images capture only a 30° to 60° FOV, whereas wide-field FA permits up to 200° FOV. The wide FOV allows visualization of the retinal vasculature. As shown in Fig. 1, peripheral vessels are captured with sufficient details. The wide FOV allows imaging of the peripheral region of retina, which makes it possible to measure the relative changes of peripheral retinal vessels.

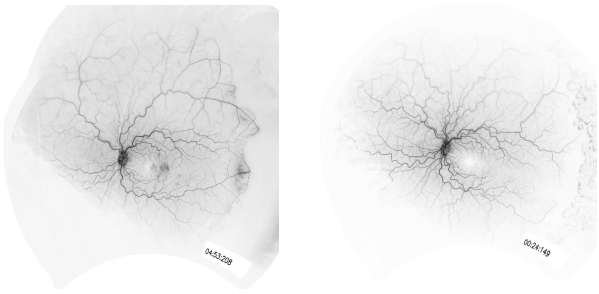

(a) (b)

Fig. 1. Sample longitudinal wide-field fluorescein angiography (FA) images for a patient taken at (a) initial visit and (b) 4 months later.

The ability to quantify RNP is important to: 1) develop a reproducible method to compare changes in RNP over time in different diseases, 2) evaluate the impact of systemic or local treatments on vessel changes over time, and 3) better understand the relationship between RNP and other ocular changes such as macular edema and visual acuity. In current clinical practice, ophthalmologists manually examine retinal images to assess RNP and changes in blood vessels occurring over time. Quantitative manual assessments in clinical setting are impractical because the processes are extremely time-consuming. Automated methods for measuring retinal vascular changes are highly desirable for providing quantitative assessments that correlate with disease/treatment progression and assist physicians in diagnosis and treatment.

Curently there are no widely accepted automated techniques for FA image analyis that quantify blood vessel changes and RNP in the retina. A preliminary approach was proposed in [**?**], which attempts to quantify the dark regions corresponding to background and non-perfused vessels. Given the relatively large regions without blood vessels, the method has limited sensitivity and does not allow for physician validation because it does not explicitly identify the non-perfused vessels. Direct quantitative measurement of vessel changes is challenging for several reasons. First, because the capture viewpoints differ between different visits, FA images need to be accurately registered before any comparison can be made. The registration, however, is not entirely trivial because of the changes in the vessels (which we are trying to quantify) and variations in time duration elapsed from the dye injection to the instant when the images are captured, which results in different vasculature appearances as the injected dye propagates in the retina.

In this paper, we propose a novel method to quantitatively measure the vasculature changes, specifically, RNP, using wide-field FA

[1]The grayscale from black to white is inverted in images presented in the paper to provide a better visualization in common display and print environments.

images captured at successive clinical visits. To overcome the aforementioned challenges, we propose a novel registration and change detection approach. The images are first independently analyzed to detect blood vessels. A pair of vessel images are then precisely registered using parametric chamfer alignment under polynomial transformation. The conventional chamfer alignment procedure is adapted to our specific problem setting to allow for changes in blood vessels between the two images. Specifically, we exploit the inherent asymmetry in the chamfer metric between the reference and target images, wherein for each point in the target binary image, the closest point in the reference binary image is considered for defining the registration error under the parametric transformation. The process is further enhanced by using a modified chamfer metric that also weights the estimated registration error for each vessel pixel in the target according to the probability that a corresponding pixel exists in the reference. The probabilities are estimated via an expectation-maximization (EM) procedure. In combination, the asymmetry and the EM based probabilistic formulation of the chamfer metric allow for mismatch between the two images arising due to both changes in vasculature and missed vessel detections.

The individual ingredients of vessel detectoin and registration that we use in our methodology have considerable existing related prior work. Vessel detection has been extensively researched for color fundus images [**?**, **?**, **?**, 3–8, 10–12], although there is relatively little work for FA imagery [17]. Existing retinal image registration methods rely on determining correspondences between images. For instance, in [14], the method for the multimodal fundus images registration is proposed using the locations of vascular bifurcations. Edge-based features [15] also have been exploited. [16] proposed a method to register wide-field FA images based on bifurcations and elongated elements. These methods are more suited for the problem of registering the multiple images taken during a single clinic visit where changes occur as the dye perfuses but are small from image to image and there is no fundamental change in the vasculature. The methods face significant challenges in aligning images from different clinical visits due to the missing correspondence and bifurcation points in one image relative to the other.

The paper is organized as follows. We describe the proposed method in Section 2 and present the experimental results in Section 3. Section 4 summarizes the concluding remarks.

2. PROPOSED METHOD

The proposed method addresses the problem of quantitatively and directly measuring retinal blood vessels to assess the clinically significant changes occurring in retinal vasculature over time. The pipeline of the proposed method is depicted in Fig. 2. It takes as input a pair of FA images for a patient captured at successive visits. Blood vessels are first extracted in the image from each visit using vessel detection method [17], as illustrated by the images labeled as "detected vessels" in Fig. 2. Using parametric chamfer alignment [18, 19], the binary vessel images are precisely registered to obtained a co-aligned pair. The chamfer alignment is performed using an EM framework, which is robust to outliers that correspond to vessels presented only in one temporal instance due to vasculature changes. The co-aligned pair identifies both common and distinct regions of vasculature and allows quantitative assessment of the changes in retinal non-perfusion.

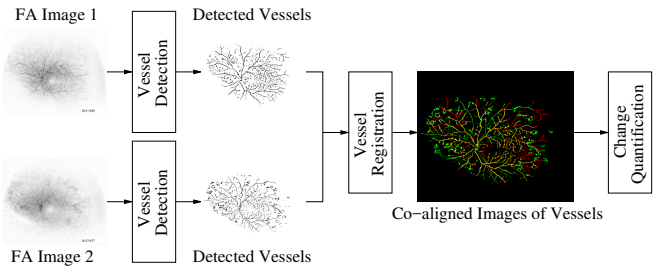

Fig. 2. Proposed methodology for measuring retinal vasculature changes using FA images.

2.1. Vessel Detection

As shown in Fig. 1, the longitudinal FA images normally differ in the capture viewpoints and in the time elapsed from the injection of the dye to the capture of the images, introducing variations in the images that do not allow for direct quantitative comparison. Therefore, the first step of the proposed method is to detect vessels from two input FA images.

The retinal blood vessels inherently exhibit variations in different orientations and changes in scales between major and minor branches. To take into account these characteristics of vessel structures, we adopt a vessel detection method [17] that uses a set of orientated modified top-hat morphological filters with multi-scale analysis. Decomposing the original FA image into multiple scales, the vessels at each scale are detected independently and then fused together to achieve the final binary vessel map. Modified morphological top-hat operators with linear structuring elements with different orientations are used to extract bright and rectilinear structures with matching orientation, which represent the shape of blood vessels in the image. Figure 3 shows the results of vessel detection for the images in Fig 1.

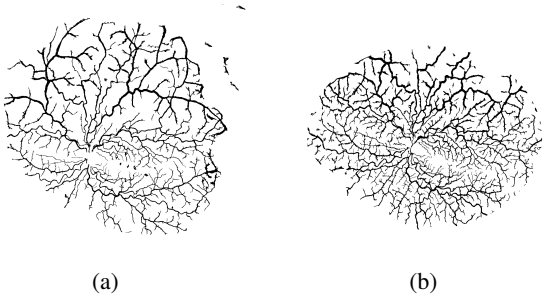

Fig. 3. Sample results of detected vessels for images shown in Fig. 1.

2.2. Retinal Image Registration

We propose to register a pair of binary vessel images obtained from Sec. 2.1 using parametric chamfer matching [18, 19]. We denote one binary vessel image as reference I_r and the other as target I_t. Let $\mathbf{P} = \{\mathbf{p}_i\}_{i=1}^{N_i}$ and $\mathbf{Q} = \{\mathbf{q}_j\}_{j=1}^{N_j}$ be two sets of points of vessel pixels in the reference and the target images, respectively, where $\mathbf{p}_i = (x_i, y_i)$ and $\mathbf{q}_j = (u_j, v_j)$. We apply the second-order polynomial transformation $\mathcal{T}_\beta$ to map target points to the reference

points. The transformation of target points, $\mathcal{T}_\beta(\mathbf{q}_j)$, is modeled as

$$\mathcal{T}_\beta(\mathbf{q}_j) = \begin{bmatrix}\beta_1\\ \beta_7\end{bmatrix} + \begin{bmatrix}\beta_2 & \beta_3\\ \beta_8 & \beta_9\end{bmatrix}\begin{bmatrix}u_j\\ v_j\end{bmatrix} + \begin{bmatrix}\beta_4 & \beta_5 & \beta_6\\ \beta_{10} & \beta_{11} & \beta_{12}\end{bmatrix}\begin{bmatrix}u_j^2\\ u_jv_j\\ v_j^2\end{bmatrix}, \tag{1}$$

where $\{\beta_i\}_{i=1}^{12}$ are the transformation parameters.

The chamfer distance, $d_j(\beta)$, between reference points $\mathbf{P}$ and each transformed target points $\mathcal{T}_\beta(\mathbf{q}_j)$ is defined as the distance between $\mathcal{T}_\beta(\mathbf{q}_j)$ and its nearest point from $\mathbf{P}$

$$d_j(\beta) = \min_i \|\mathbf{p}_i - \mathcal{T}_\beta(\mathbf{q}_j)\|^2. \tag{2}$$

The optimal registration between images I_r and I_t is achieved by determining the transformation parameters that minimizes the error metric

$$\hat{\beta} = \arg\min_\beta \frac{1}{N_j}\sum_{j=1}^{N_j} d_j(\beta), \tag{3}$$

where N_j is the number of points in the target image I_t.

Observe that chamfer matching in (3) is asymmetric: because the error is aggregated only over points in the target image, points in the reference image with no corresponding points in the target image do not contribute to the error metric. Because the changes we are interested in are manifested primarily as increases or decreases in perfusion, we exploit this asymmetry by considering both possible choices for the reference and target image allocations and choosing the one with the smaller mean chamfer distance[2]. While this is beneficial, the formulation in (3) still faces a challenge from differences that are not unidirectoinal (i.e. in only one image) and outliers. The chamfer distance of outlier points are relatively large and minimization of (3) in the presence of outliers invariably does not converge to the desired solution. To take into account the outlier points, latent variables χ_j are introduced to assess putative correspondence between point $\mathbf{q}_j$ and reference points $\mathbf{P}$, where $\chi_j = 1$ indicates $\mathbf{q}_j$ has corresponding points in $\mathbf{P}$ and is not outlier. The optimal transformation parameters $\hat{\beta}$ is then estimated by minimizing the modified error metric

$$\hat{\beta} = \arg\min_\beta \frac{1}{N_j}\sum_{j=1}^{N_j} p_j d_j(\beta), \tag{4}$$

with respect to β, where p_j is the posterior probability that χ_j is 1.

The probabilistic chamfer distance in (4) is an ideal metric for registering a pair of longitudinal FA image. The minimization of weighted sum of distance between transformed target point $\mathcal{T}_\beta(\mathbf{q}_j)$ and its nearest point from $\mathbf{P}$ results in transforming points of vessel pixels in I_t to a close proximity of the vessel pixel locations in I_r. The weights, which are defined as the posterior probability of point $\mathbf{q}_j$ being an inlier, improve robustness of registration by reducing the effects of outlier points.

We use EM algorithm [20] to determine the optimal solution $\hat{\beta}$. EM algorithm iteratively repeats between two steps, namely E-step and M-step, until convergence. In E-step, the posterior probabilities p_j are updated based on current transformation parameters. The transformed point with large chamfer distance is unlike to be inliers and thus is assigned with a low value of p_j to reduce the impact on estimating β in M-step, as indicated in (4). Given the updated p_j, we determine the optimal parameters $\hat{\beta}$ in M-step. Specifically, we use Levenberg-Marquardt (LM) iteration algorithm [21]. Starting with an initial guess β_0, β is adjusted by an updating vector δ to $\beta + \delta$ at each iteration, where δ is the solution to the equation

$$\left(\sum_{j=1}^{N_j}\mathbf{J}_j^T\mathbf{J}_j + \lambda\mathbf{I}\right)\delta = 2\sum_{j=1}^{N_j} p_j\mathbf{J}_j\mathbf{r}_j, \tag{5}$$

where $\mathbf{r}_j$ is the residual vector for point $\mathbf{p}_j$ that can be efficiently calculated by using the distance transform [22], $\mathbf{I}$ is a 12×12 identity matrix, $\mathbf{J}_j$ is the Jacobian matrix the Jacobian matrix at each transformed target point $\mathcal{T}_\beta(\mathbf{q}_j)$, which is computed as

$$\frac{\partial\mathcal{T}_\beta(\mathbf{q}_j)}{\partial\beta} = \begin{bmatrix}1 & u_j & v_j & u_j^2 & u_jv_j & v_j^2 & 0 & 0 & 0 & 0 & 0 & 0\\ 0 & 0 & 0 & 0 & 0 & 0 & 1 & u_j & v_j & u_j^2 & u_jv_j & v_j^2\end{bmatrix}. \tag{6}$$

The optimal parameters $\hat{\beta}$ returned from LM algorithm can be trapped in local minima. A good initialization is of importance to find desire solution. To do so, we perform a sequential iteration for LM algorithm. More concretely, we start with an Euclidean transformation parameterized by translation and rotation. A sequence of similarity, affine, projective (homography), and second-order polynomial transformation is then estimated using initial point that is the optimal solutions from previous step.

2.3. Change Quantification

Given the estimated parameters $\hat{\beta}$, we apply the second-order polynomial transformation to the target image I_t. Changes in retinal vessels can be quantified and visualized from the co-aligned pair.

Figure 4 shows an example illustrating the process of comparing and quantifying retinal blood vessels differences from the co-aligned pair. Fig. 4 (a) illustrates the results of alignment, obtained in Sec. 2.2, by superimposing the images as red (earlier in time) and green channels (later in time) so that common locations are identified as yellow. The co-aligned images are further processed to quantify differences of interest while ignoring minor inaccuracies in registration and variations in estimated vasculature thickness caused by other imaging parameters, such as time duration elapsed from the dye injection to the instant when the images are captured. As shown in Fig. 4 (b), regions of vasculature shown in red are identified as common, in blue as those with lost perfusion, and in green as those with added perfusion.

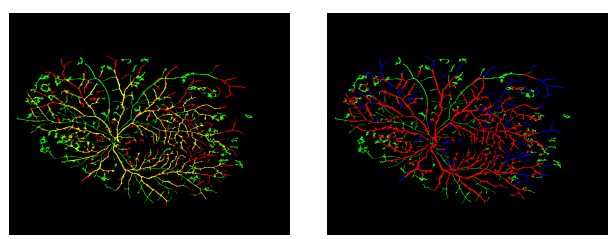

(a) (b)

Fig. 4. Example illustrating automated comparision and quantification of blood vasculature differences.

Quantitatively, the percentage increase of blood vessel perfusion K_i and percentage decrease of perfusion K_d can be calculated as

$$K_i = \frac{N_g}{N_r} \quad K_d = \frac{N_b}{N_r}, \tag{7}$$

where N_r, N_g, and N_b are the number of pixels of common region, added perfusion, and lost perfusion, respectively.

[2] Although other powerful point-based registration techniques exist (see for example [**?**] and the references therein), they typically do not exhibit this asymmetry.

3. EXPERIMENTAL VALIDATION

We identify two patients who have a large amount of RNP and collect FA images to test the performance of the proposed method. The images are captured by an Optos California camera [23] at 200° FOV. Each image is manually annotated by an ophthalmologist to provide ground truth binary vessel masks using VAMPIRE annotation tools [10]. Only two images are used in the assessment because manual annotation is rather time intensive, annotation tools notwithstanding. For the first patient (P1), regions around fovea are identified corresponding to changes in vessel perfusion, and for the second patient (P2), changes occur in peripheral regions. Figure 5 shows the fovea regions of longitudinal FA images for P1 and corresponding manually annotated binary vessel maps.

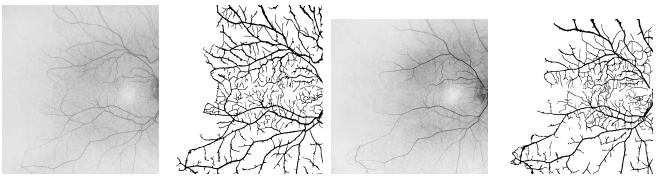

(a) (b) (c) (d)

Fig. 5. Sample ground truth vessel images. (a) and (c) show the fovea regions in the FA images where vessel changes are identified by an ophthalmologist. The images in (a) and (c) are captured at initial visit and 4 months later, respectively. (b) and (d) are manually labeled vessel maps for (a) and (c), respectively.

3.1. Quantitative And Qualitative Comparison

In our experiments, we apply the proposed method to identify and measure the changes in RNP over time and compare with ground truth in terms of the percentage increase of vessel perfusion K_i, percentage decrease of perfusion K_d, as well as the number of pixels of common region N_r, increased perfusion N_g, and lost perfusion N_g.

We choose the FA image of the initial visit as reference and the one of later visit as target. Table 1 lists the quantitative comparison in terms of the 5 aforementioned metrics for two patients. For the first patient (P1), the percentage increases K_i and decrease K_d are close to the ground truth values. The proposed method estimates 10.4% and 35.8% of increased and decreased perfusion in blood vessels, whereas ophthalmologist-provided estimates are 8.1% and 35.5%, respectively. A visual comparison for the first patient is illustration in Fig. 6 (a) and (b), which show ground truth and results of the proposed method, respectively. Regions of vasculature shown in red are identified as common, in blue as those with lost perfusion, and in green as those with increased perfusion. It can be seen that most changes are correctly identified, with the exception of some fine vessels around the fovea.

		K_i	K_d	N_r	N_g	N_b
P1	Proposed	0.104	0.358	121605	12670	43512
	GT	0.081	0.355	130498	10555	46358
P2	Proposed	0.231	0.286	87435	20230	24952
	GT	0.158	0.297	93567	14814	27794

Table 1. Quantitative results of vessel changes measurement. GT stands for ground truth.

For the second patient (P2), peripheral regions are identified as changes in vessel. Figure 6 (c) and (d) show the ground truth and the results of proposed method for this patient, respectively. We can see that both decreased and increased perfusion can be identified: most decreased perfusion happens in the right side in Fig. 6 (d) whereas increased perfusion are identified in the bottom left corner in Fig. 6 (d). The results of visual examination are accordance with that of quantitative comparison.

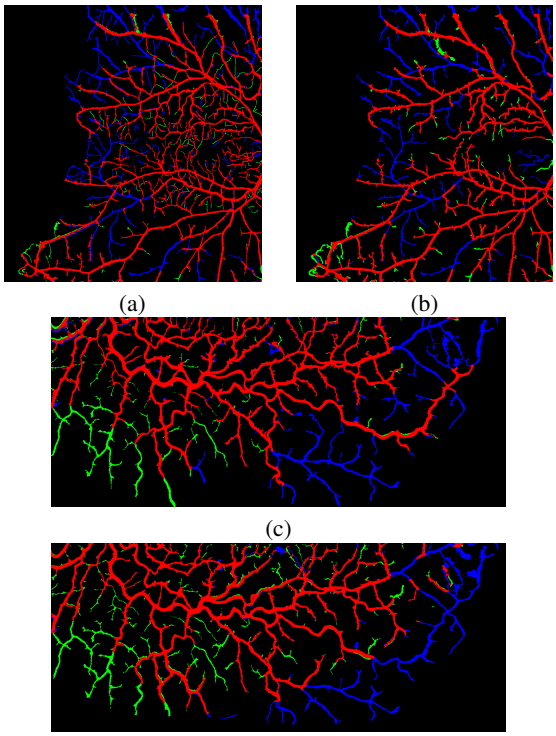

(a) (b) (c) (d)

Fig. 6. Visual comparison of vessel change detection. (a) and (c) show the ground truth for P1 and P2, respectively, and (b) and (d) show the results of proposed method for corresponding patients. The vessels in red, green, and blue are identified as common, lost perfusion, and increased perfusion, respectively.

4. CONCLUSION

We propose a method for direct quantification of longitudinal changes in retinal vessel from wide-field FA images comprising three steps: vessel detection, retinal image registration, and change quantification. The key contribution is a novel second-order polynomial transformation based parametric chamfer alignment procedure. Specifically, by using a probabilistic formulation and exploiting inherent asymmetry, the proposed chamfer alignment approach allows precise registration of FA images taken from different viewpoints and several months apart despite changes in the vascular network and variation in dye perfusion. The precision registration enables accurate automated assessment of changes. Both qualitative and quantitative results indicate that the proposed method provides accurate assessments of retinal vasculature changes that are in agreement with ophthalmologist-provided annotations.

5. ACKNOWLEDGMENT

We thank the Center for Integrated Research Computing, University of Rochester, for providing access to computational resources.

6. REFERENCES

[1] T. Y. Wong and R. McIntosh, "Systemic associations of retinal microvascular signs: a review of recent population-based studies," *Ophthalmic and Physiological Optics*, vol. 25, no. 3, pp. 195–204, 2005.

[2] A. Manivannan, J. Plskova, A. Farrow, S. Mckay, P. F. Sharp, and J. V. Forrester, "Ultra-wide-field fluorescein angiography of the ocular fundus," *Amer. J. Ophthalmology*, vol. 140, no. 3, pp. 525–527, 2005.

[3] C. L. Srinidhi, P. Aparna, and J. Rajan, "Recent advancements in retinal vessel segmentation," *J. Med. Syst.*, vol. 41, no. 4, p. 70, 2017.

[4] M. Niemeijer, J. Staal, B. Van Ginneken, M. Loog, M. D. Abramoff *et al.*, "Comparative study of retinal vessel segmentation methods on a new publicly available database," in *SPIE Medical Imaging*, vol. 5370, 2004, pp. 648–656.

[5] P. Liskowski and K. Krawiec, "Segmenting retinal blood vessels with deep neural networks," *IEEE Trans. Med. Imaging*, vol. 35, no. 11, pp. 2369–2380, Nov 2016.

[6] K.-K. Maninis, J. Pont-Tuset, P. Arbeláez, and L. Van Gool, "Deep retinal image understanding," in *Intl. Conf. Med. Image Computing and Computer-Assisted Intervention*, 2016, pp. 140–148.

[7] J. Son, S. J. Park, and K.-H. Jung, "Retinal vessel segmentation in fundoscopic images with generative adversarial networks," *arXiv:1706.09318*, 2017.

[8] S. Chaudhuri, S. Chatterjee, N. Katz, M. Nelson, and M. Goldbaum, "Detection of blood vessels in retinal images using two-dimensional matched filters," *IEEE Trans. Med. Imaging*, vol. 8, no. 3, pp. 263–269, Sep 1989.

[9] A. Hoover, V. Kouznetsova, and M. Goldbaum, "Locating blood vessels in retinal images by piecewise threshold probing of a matched filter response," *IEEE Trans. Med. Imaging*, vol. 19, no. 3, pp. 203–210, 2000.

[10] A. Perez-Rovira, K. Zutis, J. Hubschman, and E. Trucco, "Improving vessel segmentation in ultra-wide field-of-view retinal fluorescein angiograms," in *IEEE Intl. Conf. Eng. in Med. and Biol. Soc.*, 2011, pp. 2614–2617.

[11] T. A. Soomro, J. Gao, M. Paul, and L. Zheng, "Retinal blood vessel extraction method based on basic filtering schemes," *IEEE Intl. Conf. Image Proc.*, 2017.

[12] F. Zana and J. C. Klein, "Segmentation of vessel-like patterns using mathematical morphology and curvature evaluation," *IEEE Trans. Image Proc.*, vol. 10, no. 7, pp. 1010–1019, Jul 2001.

[13] E. M. Sigursson, S. Valero, J. A. Benediktsson, J. Chanussot, H. Talbot, and E. Stefánsson, "Automatic retinal vessel extraction based on directional mathematical morphology and fuzzy classification," *Patt. Recogn. Ltrs.*, vol. 47, pp. 164–171, 2014.

[14] T. E. Choe, G. Medioni, I. Cohen, A. C. Walsh, and S. R. Sadda, "2-D registration and 3-D shape inference of the retinal fundus from fluorescein images," *Med. Image Analysis*, vol. 12, no. 2, pp. 174–190, 2008.

[15] C. L. Tsai, C. Y. Li, G. Yang, and K. S. Lin, "The edge-driven dual-bootstrap iterative closest point algorithm for registration of multimodal fluorescein angiogram sequence," pp. 636–649, March 2010.

[16] A. Perez-Rovira, R. Cabido, E. Trucco, S. J. McKenna, and J. P. Hubschman, "RERBEE: Robust efficient registration via bifurcations and elongated elements applied to retinal fluorescein angiogram sequences," pp. 140–150, Jan 2012.

[17] L. Ding, A. Kuriyan, R. Ramchandran, and G. Sharma, "Multiscale morphological analysis for retinal vessel detection in wide-field fluorescein angiography," submitted to Proc. Western NY Image and Signal Proc. Wksp. 2017.

[18] H. G. Barrow, J. M. Tenenbaum, R. C. Bolles, and H. C. Wolf, "Parametric correspondence and chamfer matching: Two new techniques for image matching," in *Proc. Int. Joint Conf. Artificial Intell.*, 1977, pp. 659–663.

[19] A. Elliethy and G. Sharma, "Automatic registration of wide area motion imagery to vector road maps by exploiting vehicle detections," *IEEE Trans. Image Proc.*, vol. 25, no. 11, pp. 5304–5315, 2016.

[20] A. P. Dempster, N. M. Laird, and D. B. Rubin, "Maximum likelihood from incomplete data via the EM algorithm," *J. Roy. Statist. Soc. B (methodol.)*, pp. 1–38, 1977.

[21] J. Nocedal and S. Wright, *Numerical optimization*. Springer, 2006.

[22] G. Borgefors, "Distance transformations in digital images," *Comp. Vis., Graphics and Image Proc.*, vol. 34, no. 3, pp. 344–371, 1986.

[23] *Optos California Tech Sheet*, Optos, 2015. [Online]. Available: https://www.optos.com/globalassets/www.optos.com/products/california/california-brochure-us.pdf